Ground Experiment of Spacecraft Attitude Control Using Hardware Testbed

Choongsuk Oh* and Hyochoong Bang**
Department of Aerospace Engineering
Korea Advanced Institute of Science and Technology(KAIST)
373-1 Kusong-dong, Yusung-gu, Taejon, 305-701, Korea

Abstract

The primary objective of this study is to demonstrate ground-based experiment for the attitude control of spacecraft. A two-axis rotational simulator with a flexible arm is constructed with on-off air thrusters as actuators. The simulator is also equipped with payload pointing capability by simultaneous thruster and DC servo motor actuation. The azimuth angle is controlled by on-off thruster command while the payload elevation angle is controlled by a servo-motor. A thruster modulation technique PWM(Pulse Width Modulation) employing a time-optimal switching function plus integral error control is proposed. An optical camera is used for the purpose of pointing as well as on-board rate sensor calibration. Attitude control performance based upon the new closed-loop control law is demonstrated by ground experiment. The modified switching function turns out to be effective with improved pointing performance under external disturbance. The rate sensor calibration technique by Kalman Filter algorithm led to reduction of attitude error caused by the bias in the rate sensor output.

Key Word : Attitude control of spacecraft, Two-axis rotational simulator, Flexible arm, Thruster modulation

Introduction

Ground-based experiment for spacecraft attitude control using hardware simulators has received considerable attention during last decades[1]-[4]. There are favorable advantages in ground experiment for the evaluation of attitude control performance instead of actual spacecraft. Large spacecraft with flexible structural elements has been an intensive subject of study with numerous technical papers reported[5]-[9]. Interaction between controller and structure should be taken into account in implementation of the controllers[10],[11].

Single axis slew maneuver of flexible spacecraft has been investigated by a series of previous work. Real-time output feedback control has been applied by collocated sensor and actuator system[1],[3]. The output feedback control using Lyapunov stability theory for flexible spacecraft was proven to be robust with respect to modeling error and uncertainty[1],[3]. Reaction wheel is an appropriate actuation device generating smooth torque profile for slewing flexible spacecraft with less induced vibration. On-off thruster has been tested also in ground-based experiment[4]. A minimum-time switching function was used to form closed-loop control law[4].

A number of open-loop control strategies have been proposed which are focused on switching time optimization satisfying various terminal and boundary conditions at the end of

* Graduate Student, Department of Aerospace Engineering
** Associate Professor, Department of Aerospace Engineering
E-mail : hcbang@fdcl.kaist.ac.kr, TEL : 042-869-3722, FAX : 042-869-3710

maneuver time[5]-[9]. Robust open-loop control with switching time parameterization has been investigated[8],[9].

On-off thruster is a principal actuator in the spacecraft attitude control. The thruster is largely employed for large angle attitude maneuver instead of attitude stabilization. The major approaches for the reaction jet controller may be bang-bang and pulse modulation techniques[10],[11]. The bang-bang controller is implemented in switching function which usually requires excessive thruster action demanding much fuel consumption[4]. For this reason, time optimal bang-bang controller is not applied to practical control missions. Therefore, pulse modulators are commonly applied due to their reduced fuel consumption and quasi-linear characteristic. Thruster output is usually constant, and modulation techniques are applied to construct the given control command. Pulse modulation techniques have been developed and tested as pseudo-rate modulator, pulse width modulator(PWM), integral-pulse frequency modulator(IPFM)[10],[11] and pulse-width pulse-frequency modulator(PWPF)[12]-[15]. PWM is based upon fixed frequency with variable pulse width while the PWPF modulation adjusts both pulse width and pulse frequency[14],[15]. PWPF modulator has been used in the control systems of such spacecraft as Agena, INTELSAT V, INSAT, and ARABSAT satellites[15].

In this study, ground-based spacecraft attitude control experimental study is investigated. A closed-loop switching control law in conjunction with thruster PWM technique is attempted for the slewing maneuver of a hardware testbed. Two-axis pointing of on-board payload model is also studied. The on-board payload represents a star tracker for precision attitude determination. Closed-loop control includes a integral term in the switching function to account for the unmodeled disturbance. In addition, bias estimation of a angular rate sensor[16] using the optical payload output is demonstrated by experiment. Kalman filter algorithm is employed to identify the bias signal existing in the rate sensor output[17]. This paper therefore conveys practical results through real-time experiment of closed-loop control with a new switching function, and sensor calibration demonstration using the Kalman filter algorithm.

Ground Testbed Configuration

The actual picture of the experimental testbed with a schematic is presented in Fig. 1. The main structure consists of a rigid center body and a flexible arm attached to the center body. The center body of a disk shape representing a satellite main body is supported on top of a single-axis ball bearing. Main rotational motion takes place about the vertical axis. Moment of inertia of the

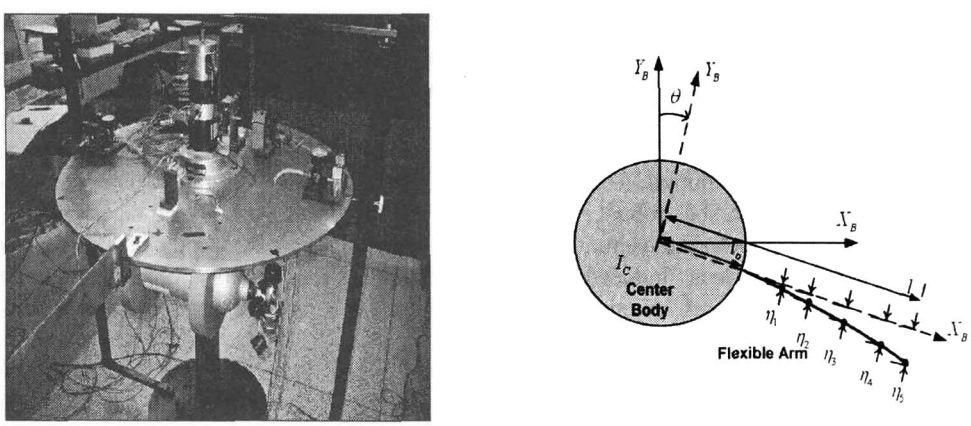

(a) (b)

Fig. 1. Configuration of the hardware simulator (a) The actual picture of the testbed (b) The discrete model consisting of a center body and a flexible arm

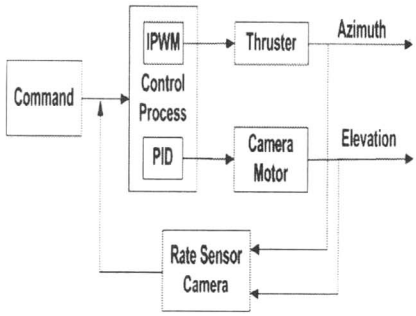

Fig. 2. Control modes of the testbed

Table 1. Testbed equipment specifications

Components	Specifications
D/A Board	A/D:16Ch, D/A:12Ch
Solenoid valve	Operational voltage -24V
Air tank	Max pressure: 3000 lbf/in^2
Regulator	Input pressure: 3000 lbf/in^2 Output pressure: 100 lbf/in^2
Encoder	Resolution 0.1deg
Testbed	Height 1m, radius 0.9m
Camera and motor	Tele8530 CCD camera Maxon 118752
Rate sensor	Bias:2.5 ± 0.245[V] Scale factor: 15mV/deg/sec

center body is about 2.32[kg-m^2]. A CCD camera payload model is mounted also on top of the center body. The payload elevation angle or line of sight is controlled by a separate motor with a driver unit. Payload line of sight is therefore controlled by the main body rotation and rotation of the payload about its body axis. The center body vertical axis rotation is governed by thrusters, while the payload module elevation angle is controlled by a dedicated servo motor. The overall control modes are explained in Fig. 2.

A reaction wheel, which is not used in this study, is driven by a DC servo motor and located at the center of the main body. Two sets of thruster modules are symmetrically arranged on both sides of the main body. The thrusters operated by solenoid valves use compressed air. Magnitude of the thrust output is estimated to be about 0.29[Nm]. Main air tanks for thrusters are located under the center body. The rotational angle of the main body can be measured by encoder while the angular rate is obtained from a rate sensor. Integrated rate output is employed for actual implementation of the controller. Specifications of the testbed components are presented in Table 1.

Flexible appendage with a tip mass is cantilevered to the main body. The flexible dynamics model for the combined rotational and flexible dynamic motions can be written as[1][3]

$$I_c \ddot{\theta} + \int_{l_0}^{l} \rho x(x\ddot{\theta} + \frac{\partial^2 y}{\partial t^2})dx + m_t l(l\ddot{\theta} + \frac{\partial^2 y}{\partial t^2}) = u \tag{1}$$

$$\rho(x\ddot{\theta} + \frac{\partial^2 y}{\partial t^2}) + EI\frac{\partial^4 y}{\partial x^4} = 0, \qquad l_0 < x < l \tag{2}$$

where I_c is moment of inertia of the center body, θ is angular position of the main body, m_t is tip mass, u is the control torque, ρ and EI are the linear mass density and elastic rigidity of the flexible arm. Furthermore, $y(x, t)$ represents deflection of the flexible arm, l_0 represents radius of the center body, and l is distance from the testbed center to the tip of the flexible appendage. The governing differential equations of motion are hybrid equations; ordinary and partial differential equations from the center body rotation and flexible arm deflection. Disturbance is produced by the flexible arm attached to center body and static friction from bearing. Flexible arm dynamics also satisfy boundary conditions at the root and tip of the arm such as[3]

$$y(x, t) = \frac{\partial y}{\partial x} = 0 \quad at \quad x = l_0 \tag{3}$$

$$EI\frac{\partial^2 y}{\partial x^2} = 0, \; EI\frac{\partial^3 y}{\partial x^3} = m_t(l\ddot{\theta} + \frac{\partial^2 y}{\partial t^2}) \quad at \quad x = l \tag{4}$$

The torque equilibrium equation also can be rewritten as

$$I_t \ddot{\theta} + \int_{l_0}^{l} \rho x \frac{\partial^2 y}{\partial t^2} dx + m_t l \frac{\partial^2 y}{\partial t^2} \Big|_{l} = u \tag{5}$$

where I_t represents the total rigid moment of inertia.

$$I_t = I_c + \int_{l_0}^{l} \rho x^2 dx + m_t l^2 \tag{6}$$

The original hybrid differential equations of motion can be discretized into a finite dimensional mathematical model[18]. The mathematical model is developed for simulation study and dynamic analysis purpose. The finite element method for the typical beam bending motion is applied to yield[16]

$$\begin{bmatrix} I_t & M_{\theta\eta} \\ M_{\eta\theta} & M_{\eta\eta} \end{bmatrix} \begin{bmatrix} \ddot{\theta} \\ \ddot{\eta} \end{bmatrix} + \begin{bmatrix} 0 & 0 \\ 0 & K_{\eta\eta} \end{bmatrix} \begin{bmatrix} \theta \\ \eta \end{bmatrix} = \begin{bmatrix} 1 \\ 0 \end{bmatrix} u \tag{7}$$

Elements of the mass and stiffness matrices are computed from finite element approximation, and flexible degree of freedom(η) includes deflection and rotation of the nodal point of each finite element[16]. Equation (7) also can be rewritten in a matrix form as

$$M\ddot{q} + D\dot{q} + Kq = Fu \qquad q = [\theta \ \eta]^T \tag{8}$$

where M and K are mass and stiffness matrices, respectively, and the dissipative damping matrix D is added to account for damping effect of the flexible beam. State space form of the second order differential equations of motion can be written as

$$\dot{x} = Ax + Bu \tag{9}$$

$$y = Cx + Du \tag{10}$$

where the state vector is defined as $x = [\theta, \eta, \dot{\theta}, \dot{\eta}]$. Five flexible modes are retained in the mathematical model. Parameter settings for the proposed controller are verified by simulation and analysis using MATLAB software and mathematical model.

Attitude Control with PWM Modulator

Various thruster modulation techniques have emerged during last decades, and some of them are implemented on the actual spacecraft[12][15]. Of the modulation techniques, the PWPF(Pulse Width and Pulse Frequency) and PWM(Pulse Width Modulation) are most general ones. Analog implementation of the PWPF modulator is straightforward due to the inherent characteristics of analog electronics technology. The device is a first-order lag filter and a Schmidt trigger inside a feedback loop[14],[15]. However, PWPF modulation poses a problem associated with on-board digital microprocessors because the on-board computer sends control command at regular time intervals. Therefore, the pulse frequency modulation is not easy implement[14]. Controller design in this study is based upon the fixed frequency based PWM technique with a closed-loop switching function.

In order to provide basic background for the controller design in this study, the following Lyapunov function candidate is proposed[1],[3].

$$2U = I_c \dot{\theta}^2 + \int_{l_0}^{l} \rho (x\dot{\theta} + \frac{\partial y}{\partial t})^2 dx + \int_{l_0}^{l} \rho (EI \frac{\partial^2 y}{\partial x^2})^2 dx + m_t (l\dot{\theta} + \frac{\partial y}{\partial t})^2 + K_p (\theta - \theta_f)^2 \tag{11}$$

where $K_p > 0$ is a constant so that $U \geq 0$. The Lyapunov function is a weighted combination of each sub-system energy, and attitude error energy with respect to an equilibrium point

$$(y, \dot{y}, \theta, \dot{\theta}) = (0, 0, \theta_f, 0)$$

where θ_f is final attitude angle of the whole system. The Lyapunov function and associated controller design have been investigated extensively in a series of previous studies[1],[3],[4]. Time derivative of the Lyapunov function with the governing equations of motion and boundary conditions in (1) and (2) yields

$$\dot{U} = [u + K_p(\theta - \theta_f)]\,\dot{\theta} \tag{12}$$

A simple choice of a linear controller design results in the following result

$$u(t) = -K_p(\theta - \theta_f) - K_d\,\dot{\theta} \tag{13}$$

where $K_d < 0$ is another design parameter for which $\dot{U} = -K_d\,\dot{\theta}^2 \leq 0$. The control law in (13) is a typical PD controller in terms of the center body angular information. There is no need for direct measurement of flexible arm motion. Stability of the closed-loop system is guaranteed irrespective of modeling errors in the Lyapunov sense. The controller is therefore robust, and also easy-to-implement[1],[3]. The control command is continuous so that similar type actuators are needed to constitute a complete system. Ground-based experiment for the control law in (13) using reaction wheel type actuator is reported in detail in [1],[3]. For thruster actuator with fixed output, the control law needs to be modified. First, the original governing equations of motion is assumed to be approximated as

$$I_t\ddot{\theta} \fallingdotseq u \tag{14}$$

For the approximated system modeled by pure rigid motion, the closed-loop time-optimal switching control law is[4]

$$u(t) = -N\,sign(S(t;\,\theta,\,\dot{\theta})) \tag{15}$$

where $sign(f) = 1$ if $f > 0$, -1 if $f < 0$ is the *signum* function, and the switching function is expressed as

$$S(t;\,\theta,\,\dot{\theta}) = (\theta - \theta_f) + \gamma\frac{I_t}{2N}\,\dot{\theta}\,|\dot{\theta}| \tag{16}$$

A Dead Zone(DZ) can be augmented with the switching controller to minimize chattering effect due to the *signum* function across zero-crossing line of the switching function. The new parameter γ is introduced to compensate for potential modeling error in estimating the parameters I_t and N [4]. The controller in (16) has been demonstrated through ground experiment. Rigorous stability argument can be applied in the same context as the continuous controller case. It is well known that the minimum-time switching controller in (16) is subject to excessive fuel consumption problem due to frequent switching action. The switching action may cause fuel consumption as well as degradation of the thruster performance.

PWM is a principal modulation technique for on-board spacecraft thrusters[14],[15]. In order to circumvent disadvantage of the simple switching controller, the PWM approach based on the minimum-time switching function is introduced. The original switching function is modified by including an integral control term. The integral term is targeted to handle steady-state error due to external disturbance. Hence, modified switching function including the integral control term is given by

$$S_I(t;\,\theta,\,\dot{\theta}) = (\theta - \theta_f) + \gamma\frac{I_t}{2N}\,\dot{\theta}\,|\dot{\theta}| + K_i\int(\theta - \theta_f)\,dt \tag{17}$$

The block diagram representation of the proposed controller is presented in Fig. 3. In a rigorous sense, the new control law combines advantage of the time optimal control in response time with the PWM for fuel saving. The controller preserves robustness since the control parameters consist of center body angle and angular rate only, to which the actuator directly responds. According to the principle of the PWM, the activated reaction pulse width is adjusted in proportion to the magnitude of the torque command input.

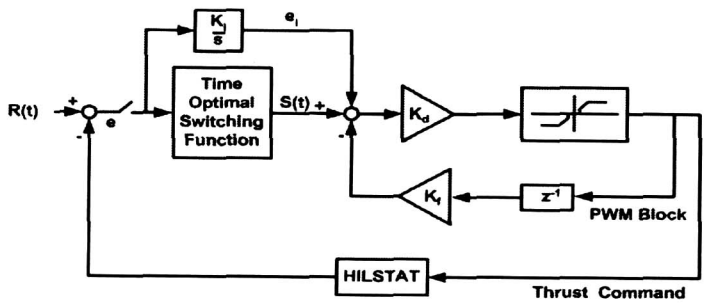

Fig. 3. Control with IPWM modulator

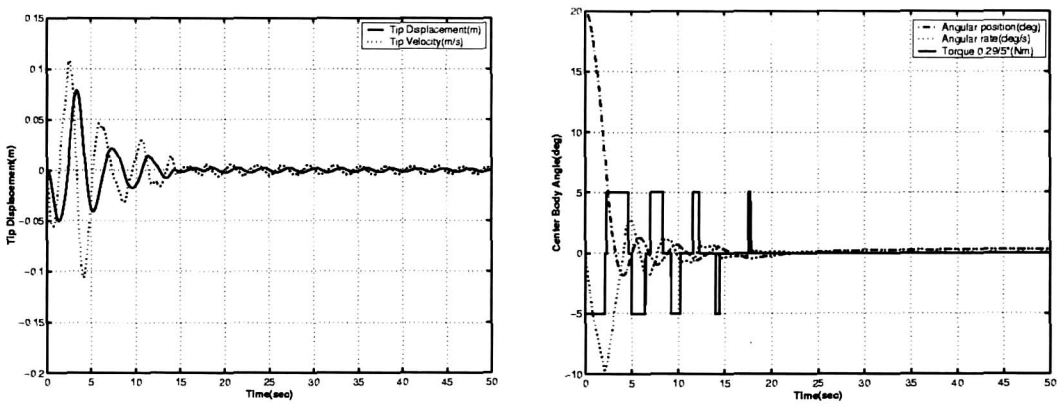

(a) (b)

Fig. 4. PWM simulation with DZ equal to 0.0067 : (a) Tip displacement, velocity (b) Center body angle, rate

In Fig. 3, the delay in the feedback loop introduces damping to the system; maximum damping occurs when the feedback signal is smaller than the PWM input. If the input signal is not greater than the feedback signal, the modulator may limit cycle itself. This criterion enables the designer to determine the feedback gain, K_f . The feed-forward gain, K_d , is selected by the minimum pulse criterion[15]. If the integral gain, K_i , is too large, the position oscillates in the steady state. Therefore, the integral gain, K_i , is chosen by trial and error procedure. As soon as thruster is turned on, the integral term is reset to zero and the integrated error signal becomes activated. Generally speaking, PWM performance is limited by the minimum and maximum pulse widths over the sampling period. Maximum pulse width is equal to the sampling period. In this research, the maximum pulse width or sampling period is set to 0.02[sec] while the minimum pulse width is 0.0067[sec] or 0.004[sec]. Simulation results for the proposed control law are shown in Figs. 4, 5, and 6. Figs. 4 and 5 present PWM simulation results without the integral control term. Positive effect of integral control action is highlighted in Fig. 6. Simulations for the PWM with the conventional switching function are conducted for two cases with different dead zones(DZs). The dead zone for Fig. 4 is equal to 0.0067 and 0.004 for Fig. 5. As it can be shown the smaller the dead zone, the better pointing accuracy is resulted. The pointing error from simulation results are summarized in Table 2. Although the thrust operating time is shortest in the PWM(DZ=0.0067), the pointing accuracy is not so satisfactory. The PWM with DZ equal to 0.004 shows good pointing accuracy, but it ends up with longer thrust operating time. However, the new controller with integral control term results in fine pointing accuracy and short thrust operating time. The unmodeled

Table 2. PWM, IPWM Simulation result

Properties	Thruster operating time	Pointing accuracy
PWM (DZ:0.0067)	6.133(sec)	0.3(deg)
PWM (DZ:0.004)	6.780(sec)	0.1(deg)
IPWM (DZ:0.0067)	6.2533(sec)	0.02(deg)

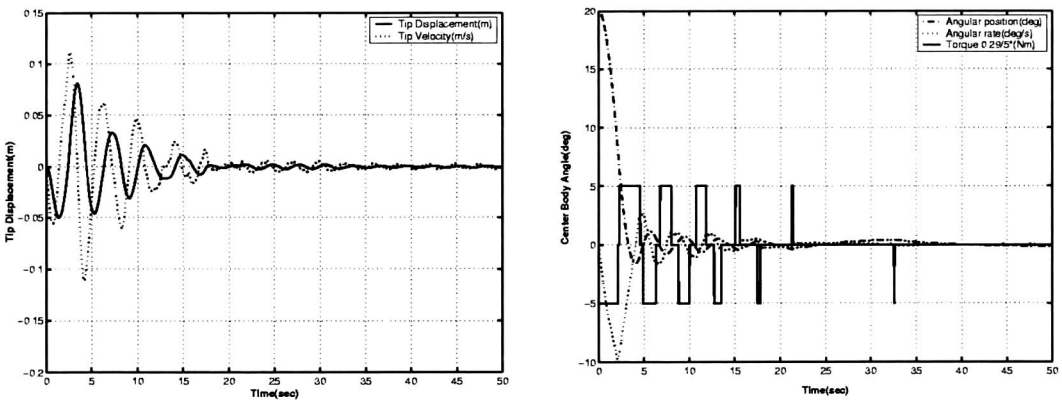

(a) (b)

Fig. 5. PWM simulation with DZ equal to 0.004 : (a) Tip displacement, velocity (b) Center body angle, rate

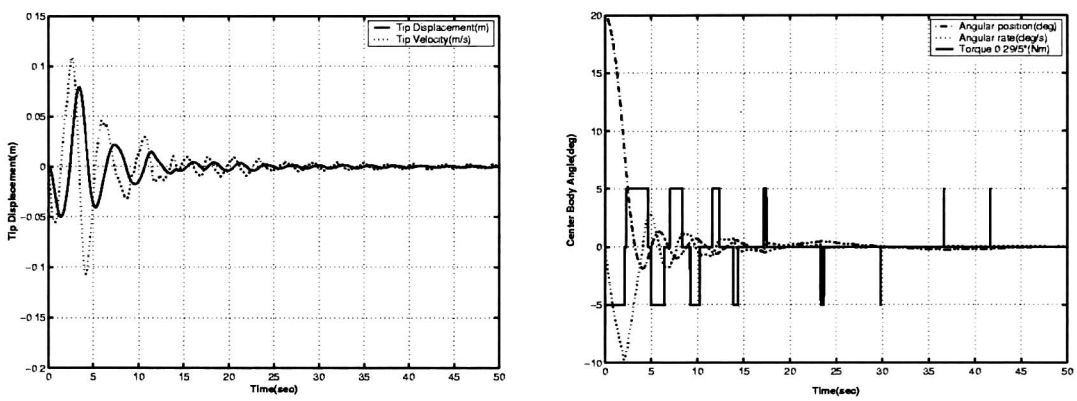

(a) (b)

Fig. 6. IPWM simulation with DZ equal to 0.0067 : (a) Tip displacement, velocity (b) Center body angle, rate

dynamics, in particular, the friction disturbance produces unnecessary thruster firing for the PWM with time-optimal switching function. The pointing performance is degraded by disturbance while the thrusters continue firings to overcome disturbance. New control command with integral term relies on integrated error signal. Steady error signal is accumulated and cause thruster firings. In this case, the fundamental principle of integral control contributes to

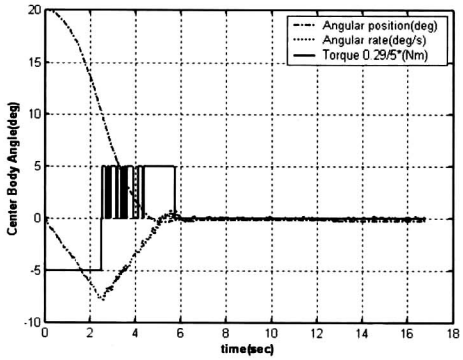

Fig. 7. PWM test with DZ equal to 0.0067

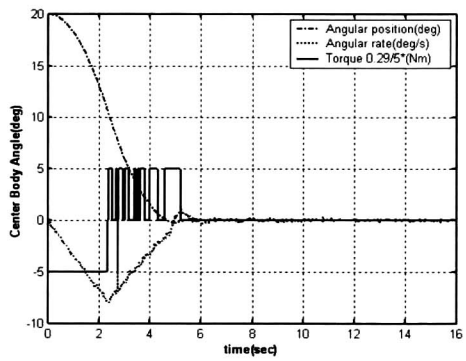

Fig. 8. PWM test with DZ equal to 0.004

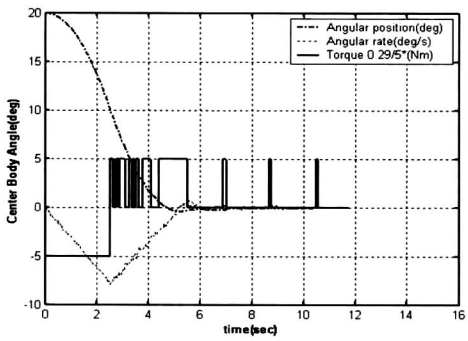

Fig. 9. IPWM test with DZ equal to 0.0067

Table 3. PWM, IPWM Experimental result

Properties	Thruster operating time	Pointing accuracy
PWM (DZ:0.0067)	3.3467(sec)	0.3(deg)
PWM (DZ:0.004)	3.5000(sec)	0.1(deg)
IPWM (DZ:0.0067)	3.4667(sec)	0.05(deg)

reduce steady error due to static friction of the center body rotation. Consequently, the thruster firing is reduced compared to regular switching function without the integral control term. Fig. 7-9 illustrate experimental results for the proposed control law. Tests are performed under conditions identical to those for simulations for comparison of results. The actual settling time is different from the simulation, due to the friction. However, similar trends are observed in that the PWM with integral control results in shorter thruster operating time with better pointing accuracy. The test results are summarized in Table 3. For PWM controller case, as the dead zone becomes shorter, pointing accuracy increases at the cost of thruster operating time.

Two-Axis Pointing Maneuver

In this section, payload pointing experiment by simultaneous control of the center body angle and the payload line of sight is investigated. A CCD camera type optical paylaod is mounted on top of the center body. The line of sight or elevation angle of the payload is controlled by a separate servo motor. A point target source is located in front of the camera field of view. Initial off-set of the target source from the center of the camera image plane is controlled by feedback control. The payload represents a star tracker which is used for the precision attitude determination of spacecraft. The point source, therefore, could be regarded as a star in the space. The point source image on the two dimensional camera plane provides attitude information of the payload line of sight. Attitude information from the camera is utilized for rate sensor bias estimation as well as simultaneous pointing of the payload axis[17].

1. Rate sensor bias estimation

First the payload is used to estimate bias of the rate sensor output signal. As presented in

Table 4. Rate sensor specifications

Specifications	Value
Range	±100 °/sec
Scale factor	15mV/ °/sec
Bias(initial offset)	+2.5±0.045VDC
Bias stability(short)	≤0.05 °/sec
Bias stability(long)	≤1.0 °/sec
Output noise	≤0.05 °/Hz
Resolution	≤0.05 °/sec

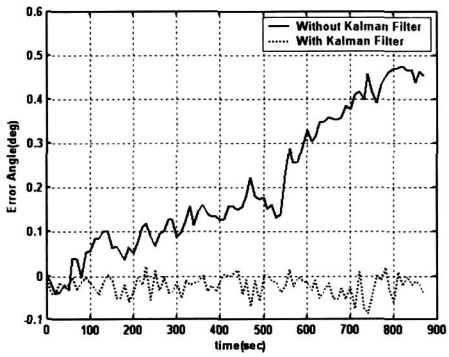

Fig. 10. Rate sensor calibration result by using the CCD camera

Table 4, the rate sensor output is mixed with bias and noise components. In majority of spacecraft precision attitude determination system, star trackers are used to estimate gyro bias[18]. Similar approach is attempted herein by ground experiment. The overall algorithm is much simplified, however, since only single-axis information is processed in contrast to the general three-axis case[18].

Kalman filter estimation algorithm is employed for sequential estimation of the bias signal. For Kalman filter implementation, the rate sensor bias is considered as Gaussian random walk process. Typical rate sensor bias modeling follows as

$$\begin{aligned} \dot{\theta}_r &= \varepsilon_r \\ \dot{\varepsilon}_r &= w \end{aligned} \tag{18}$$

where θ_r is error angle, ε_r is rate sensor bias, and ω represents white noise of constant covariance. The matrix equivalent formulation of (18) is written as

$$\begin{bmatrix} \dot{\theta}_r \\ \dot{\varepsilon}_r \end{bmatrix} = \begin{bmatrix} 0 & 1 \\ 0 & 0 \end{bmatrix} \begin{bmatrix} \theta_r \\ \varepsilon_r \end{bmatrix} = \begin{bmatrix} 0 \\ 1 \end{bmatrix} w \tag{19}$$

Introducing the state vector as

$$x = \begin{bmatrix} \theta_r \\ \varepsilon_r \end{bmatrix} \tag{20}$$

discrete state equation for discrete Kalman filter can be represented as

$$x_{k+1} = \begin{bmatrix} 1 & T \\ 0 & 1 \end{bmatrix} x_k + \begin{bmatrix} 0 \\ 1 \end{bmatrix} w \tag{21}$$

where T is the sampling interval. The measurement output is error between integrated gyro output and output from the CCD camera which is converted into angular displacement. The CCD camera image plane has 640×480 pixels so that the angle from the center of the plane to the target point is calculated as

$$\theta_x = \frac{FOV_a}{640}(x_p - 320) \tag{22}$$

$$\theta_y = \frac{FOV_e}{480}(y_p - 240) \tag{23}$$

where θ_x is azimuth angle, θ_y is elevation angle, x_p and y_p represent (x, y) position of the target in terms of number of pixels, and $FOV_a(FOV_e)$ denote field of view of the camera about azimuth(elevation) axis, respectively. The output measurement equation can be written as

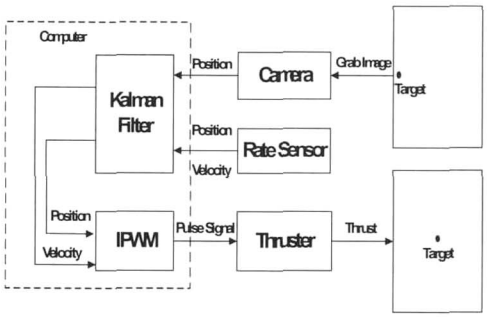

Fig. 11. Azimuth zxis control loop

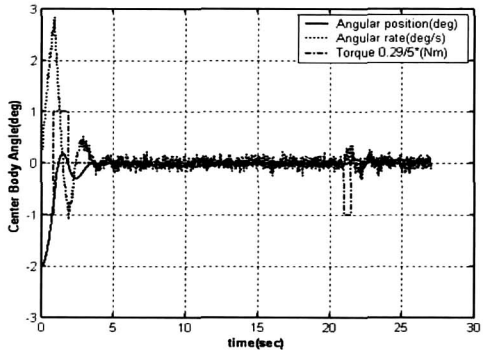

Fig. 12. Azimuth axis test result

$$z_k = [\ 1\ \ 0]\, x_k + v_k \tag{24}$$

where the z_k is the measurement, and v_k is the measurement noise at the k-th step. The noise covariance matrices of the system and the measurement are estimated as

$$E\{w_k\, w_k{}^T\} = Q_k = \begin{bmatrix} 0.00002\,\mathrm{deg}^2 s^2 & 0.001568\,\mathrm{deg}^2 s \\ 0.001568\,\mathrm{deg}^2 s & 0.156800\,\mathrm{deg}^2 \end{bmatrix} \times 10^{-6}$$

$$E\{v_k\, v_k{}^T\} = R_k = [\,(0.041\ \mathrm{deg}/s)^2\,]$$

Discrete Kalman filter logic is implemented to estimate the rate sensor bias, and estimated bias is used to update the rate sensor output. Result of the Kalman filter run for bias estimation is presented in Fig. 10. As it can be shown in Fig. 10, the error angle gradually increases up to 0.4[deg] when the calibration process is not applied. However, the steady-state error angle remains within about 0.1[deg] for 850[sec] processing time with bias estimation applied. Therefore, the optical payload, equivalent to a star tracker, demonstrates the attitude determination capability through rate sensor bias estimation.

In the following, rate sensor calibration technique is extended into the payload pointing maneuver. The off-set in CCD camera image plane is adopted as a control variable. Azimuth(vertical) and elevation(payload) axes control performance has been tested separately and in combination.

2. Control about azimuth axis

As explained already, payload azimuth angle is controlled by the center body and/or thrusters. Point source image on the CCD camera image plane provides azimuth error angle from calibrated rate sensor output as Eq. (22) indicates. Fig. 11 illustrates the azimuth axis control loop. The Kalman filter loop in Fig. 11 is activated at the earlier stage of calibration, after which the position and velocity are obtained from the rate sensor during control phase. The thruster modulation technique explained earlier is applied again with experimental results presented in Fig. 12. The commanded angular range about azimuth axis is limited to 5[deg](-2.5~+2.5) due to the camera field of view and distance from the camera to the point source. Similar results to the previous cases for the new controller with enhanced pointing accuracy are observed. In this case, the attitude determination is added to form a complete control strategy.

3. Elevation axis control

Fig. 13 shows the elevation or payload axis control loop. The elevation axis command angle range is limited to 3.8[deg] (-1.9~+1.9) as a consequence of the limited camera field of

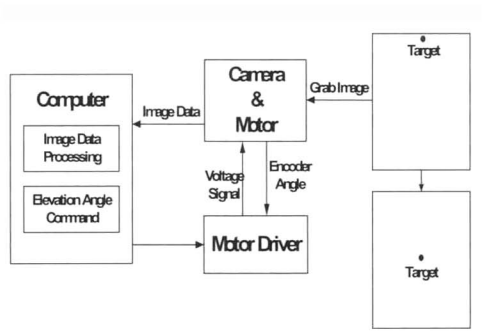

Fig. 13. Elevation axis control loop

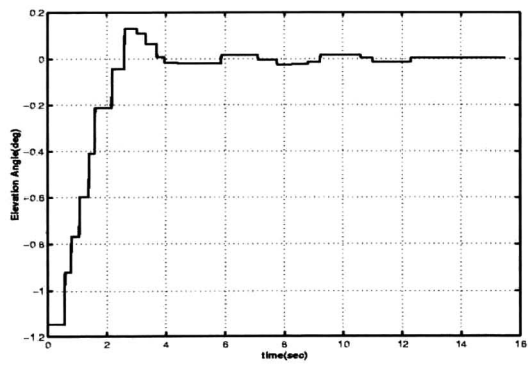

Fig. 14. Elevation axis experiment result

view. The elevation axis is controlled by a DC motor for which the motor driver is operated by own PID controller. Once the camera acquire the point source image data, elevation error angle is calculated to construct motor command to track the reference angle. The resultant motor actuation causes the initial target point image to move to the center of the camera image plane as illustrated in Fig. 14.

4. Two-axis control experiment

Simultaneous control of both azimuth and elevation axes is tested. The point source is positioned from the camera center point in both axes. Thrusters and payload control motor are activated in parallel to eliminate the initial off-set error of the point source in the camera image plane. The experimental results are shown in Fig. 15. Fig. 15 illustrates the sequential camera images at 0, 2, 3, and 5 seconds during the two-axis pointing maneuver. White-marked point source converges to the center point in about 5 sec by simultaneous maneuver in azimuth and elevation axes. The final pointing accuracy turns out to be quite satisfactory. Higher angular resolution is achieved by using the target source image on the payload image plane.

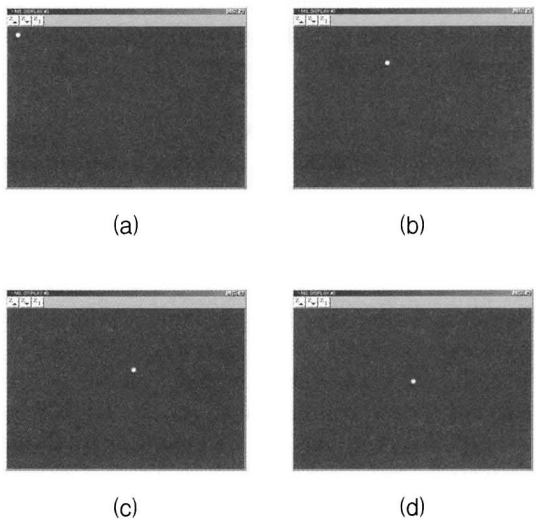

Fig. 15. Two-axis pointing experimental results : (a) 0 sec (b) 2 sec (c) 3 sec (d) 5 sec

Conclusion

Ground experiment of spacecraft attitude control using a hardware testbed is conducted with satisfactory results. The new control law with modified switching function with integral control and the PWM thruster modulation technique demonstrated enhanced performance. Reduced fuel consumption and improved pointing accuracy would be the primary benefit derived from the proposed controller. Simple output feedback law replacing complicated mathematical model-based control laws for flexible structures has been proven again. Rigorous stability argument is presented by using Lyapunov function. A CCD camera payload is used to estimate the rate sensor bias with bounded angular error. Kalman filter algorithm was applied to rate sensor bias estimation within reasonable run time. Two-axis pointing maneuver for the payload line of sight pointing is also demonstrated with experimental results. Simple algorithm but supported by actual experimental results presented in this study may provide useful guideline in spacecraft attitude control systems design and test.

Acknowledgement

This work was supported by Korea Research Foundation Grant (R02-2000-00323).

References

1. Fujii, H., Ohtsuka, T., and Udou, S., Mission Function Control of Slew Manevuer Experiment", *Journal of Guidance, Control, and Dynamics*, Vol. 12, No. 6, 1989, pp. 858-865.

2. Frangos, C., Control System Analysis of a Hardware-In-the-Loop simulation", *IEEE Trans. on Aerospace and Electronics System*, Vol. 26, No. 4, 1990, pp. 666-668.

3. Junkins, J. L., Rahman, Z., Bang, H., and Hecht, N., Near-Minimum-Time Control of Distributed Parameter Systems :Analytical and Experimental Results , *Journal of Guidance, Control and Dynamics*, Vol. 14, No. 2, 1991, pp. 406-415.

4. Agrawal, B.N. and Bang, H., "Robust Closed-loop Control Design for Spacecraft Maneuver using On-off Thrusters", *Journal of Guidance, Control, and Dynamics*, Vol.18, No.6, pp.1336-1349, 1995.

5. VanderVelde, W., and He, J., Design of Space Structure Control Systems using On-off Thrusters", *Journal of Guidance, Control, and Dynamics*, Vol. 6, No. 1, 1983, pp. 759-775.

6. Singh, G., Kabamba, P., and McClamroch, N., Planar Time Optimal Slewing Maneuvers of Flexible Spacecraft", *Journal of Guidance, Control, and Dynamics*, Vol. 12, No. 1, 1989, pp. 71-81.

7. Singhose, W., Pao, L., and Seering, W., Time-Optimal Rest-to-Rest Slewing of Multi-Mode Flexible Spacecraft using ZVD Robustness Constraints", AIAA Paper 96-3845, Aug. 1996.

8. Wie, B., Shinha R., and Liu, Q., Robust Time-Optimal Control of Uncertain Structural Systems", *Journal of Guidance, Control, and Dynamics*, Vol. 16, No. 5, 1993, pp. 980-982.

9. Liu, Q., and Wie, B., Robust Time-Optimal Control of Uncertain Flexible Spacecraft", *Journal of Guidance, Control, and Dynamics*, Vol. 15, No. 3, 1992, pp. 597-604.

10. Clark, R.N., and Franklin, G. F., Limit Cycle Oscillations in Pulse Modulated Systems", *Journal of Spacecraft and Rockets*, Vol. 6. No. 7, 1969, pp. 799-804.

11. Hablani, H. B., Multiaxis Tracking and Attitude Control of Flexible Spacecraft with Reaction Jets", *Journal of Guidance, Control and Dynamics*, Vol. 17, No. 4, 1994, pp. 831-839.

12. Anthony, T., Wie, B., and Carroll, S., Pulse-Modulated Control Synthesis for a

Flexible Spacecraft", *Journal of Guidance, Control and Dynamics*, Vol. 13, No. 6, 1990, pp. 1014-1015.

13. Song, G, Buck, N. V., and Agrawal, B. N., Spacecraft Vibration Reduction Using Pulse-Width Pulse-Frequency Modulated Input Shaper", *Journal of Guidance, Control and Dynamics, Vol.* 22, No. 3, 1999, pp. 433-440.

14. Sidi, M. J., *Spacecraft Dynamics & Control*, Cambridge, 1997.

15. Wie, B., *Spacecraft Dynamics and Control : Applications of Dynamical Systems Theory*, AIAA Educational Series, 1995.

16. Kwon, Y., and Bang, H., *The Finite Element Method using MATLAB, CRC Press*, 2000.

17. Chung, H., Ojeda, L., Borenstein, J., Accurate Mobile Robot Dead-Reckoning with a Precision-Calibrated Fiber-Optic Gyroscope , *IEEE Trans. Robot. Automat*, Vol. 17, No.1, 2001, pp.80-84.

18. Lefferts, E.J., Markley, F.L., and Shuster, M.D., Kalman Filtering for Spacecraft Attitude Estimation", *Journal of Guidance and Control*, Vol. 5, No. 5, 1982, pp. 417-429.

19. Talebi, H.A., Khorasani, K., and Patel, R.V., Neural network based control schemes for flexible-link manipulators: simulations and experiments", *Neural Networks*, 11, 1998, pp. 1357-1377.

20. Magnus Norgaard, *Neural Network Based Control System Design Toolkit*, Technical University of Denmark, 1995.

21. Karl J. Astrom, Bjorn Wittenmark, *Adaptive Control*, Addison Wesley, 1995.

22. Lewis F. L., Jagannathan S., Yesildirek A., *Neural Network Control of Robot Manipulators and Nonlinear Systems*, Taylor & Francis, 1999.